American Mineralogist, Volume 68, pages 595–603, 1983

High-pressure and high-temperature crystallographic study of the gillespite I–II phase transition

ROBERT M. HAZEN AND LARRY W. FINGER

Geophysical Laboratory, Carnegie Institution of Washington
Washington, D.C. 20008

Abstract

Crystal structures of gillespite, $BaFeSi_4O_{10}$, which has a reversible first-order phase transition at 18 kbar, were refined from data collected at 1 bar and 9, 21, and 45 kbar. Silicate-layer topology is constant through the transition, but coordination of barium increases from 8 to 10. The almost perfect square-planar coordination group of iron in gillespite I (Fe–O = 1.98Å) changes to a flattened tetrahedron with two additional long Fe–O bonds (~3Å) in gillespite II. The volume discontinuity at the gillespite I–II transition is best described as a consequence of the increased coordination of barium and iron.

Unit-cell parameters of gillespite were measured under nine high-pressure and fourteen combined high-pressure, high-temperature (*PT*) conditions. The Clausius–Clapeyron slope of the transition is 27±9 bar/°C, which is similar to the slope of gillespite-I isochores. On the basis of these observations, the behavior of the gillespite I–II transition is consistent with a geometrically controlled phase transformation, in which the size of the barium site is the critical dimensional factor.

Introduction

The barium-iron silicate gillespite ($BaFeSi_4O_{10}$), though a rare mineral, has been the subject of much research, due to both an unusual square-planar coordination of ferrous iron and to a high-pressure phase transition, the latter characterized by a striking red-to-blue color change. Strens (1966) first described the transition, which was subsequently examined by absorption spectroscopy (Abu-Eid *et al.*, 1973) and Mössbauer spectroscopy (Huggins *et al.*, 1975, 1976). Hazen and Burnham (1974, 1975) and Hazen (1977), employing high-pressure, single-crystal X-ray diffraction techniques, were successful in identifying a change from tetragonal to orthorhombic symmetry at the phase transition and an associated distortion of the iron site from ideal square-planar coordination. Hazen (1977) also discussed mechanisms of the first-order transition (ΔV = 1%) and modes of twinning induced by the reduction of symmetry at high pressure.

Gillespite I is tetragonal, $P4/ncc$, a = 7.516, c = 16.076Å, Z = 4. The structure (Fig. 1) has an 8Å subcell parallel to c, but alternate left- and right-handed rotations of four-membered silicate tetrahedral rings cause the c-dimension to be doubled to 16Å (Hazen and Burnham, 1974). Four nonbridging oxygen (O3) atoms surround each ferrous iron in almost perfect square-planar coordination. The layers of tetrahedrally coordinated silicon are linked by barium atoms in eight-fold distorted cubic coordination.

"Gillespite II"[1] is orthorhombic, $P2_12_12$, $a \cong b \cong 7.4$Å, $c \cong 7.9$Å, Z = 2, and differs from the room-pressure phase in that all four-membered rings in adjacent silicate layers have the same rotational sense. One consequence of the change in relative layer orientation is that the coordination polyhedra of both iron and barium are altered. Details of these changes were poorly resolved in the previous study of the structure at high pressure, due to the low precision of the refinement.

Several questions regarding the gillespite I–II transition remain unresolved. Hazen and Burnham's single high-pressure refinement of gillespite II, which was the first silicate structure to be determined from single-crystal, high-pressure data, is inadequate both in precision and in the number of pressures studied for calculation of polyhedral distortions and compressibilities. The pressure of the natural gillespite transition was uncertain, because internal pressure standards were not available to them. All previous experiments were performed at room temperature; thus the Clausius–Clapeyron slope of the gillespite I–II transition is also unknown. Other unresolved aspects of gillespite at high pressure are the origin of an extra absorption doublet in Mössbauer spectra of synthetic

[1] "Gillespite II," the high-pressure form of $BaFeSi_4O_{10}$, has not been observed in nature and thus is not a proper mineral name. This name has been used for convenience only.

0003–004X/83/0506–0595$02.00

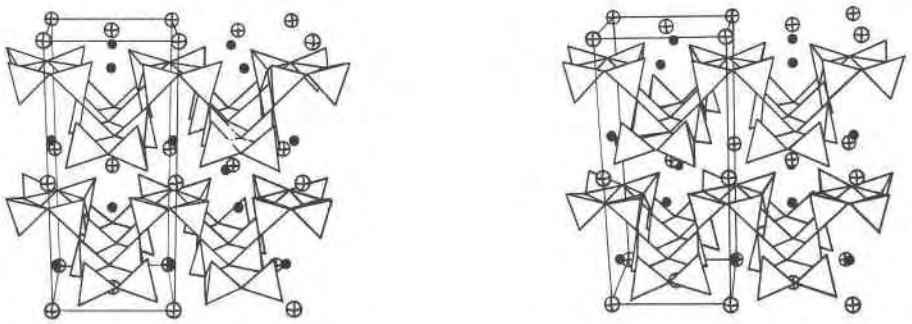

Fig. 1. Stereoscopic pair of the gillespite I crystal structure, from Hazen and Burnham (1974). Barium atoms are represented by crossed circles, iron atoms by solid circles, and oxygen atoms by the corners of silicon tetrahedra. Corner-linked tetrahedra form infinite sheets in the (001) plane. The tetragonal c axis is vertical.

$BaFeSi_4O_{10}$, and the nature of a possible third phase, "gillespite III," above 70 kbar (Huggins *et al.*, 1976).

The objectives of this study were to apply improved high-pressure, single-crystal, X-ray diffraction techniques and recently developed combined high-pressure, high-temperature (*PT*) X-ray techniques to determine polyhedral compressibilities of barium and iron in gillespite I and II, to measure the variation of gillespite lattice parameters versus temperature and pressure, to define the stability fields of gillespite I and II, and to resolve the apparent anomalies of gillespite high-pressure Mössbauer spectra.

Experimental procedures

Specimen description

The specimen of natural gillespite from Fresno County, California (Harvard University Mineralogical Collection No. 107555), was from the same sample used in previous X-ray experiments (Hazen and Burnham, 1974). Synthetic single crystals are not available; however, the only significant deviation in this natural sample from the ideal composition ($BaFeSi_4O_{10}$) is 0.2 wt.% TiO_2, corresponding to approximately 0.01 Ti atom per Fe.

High-pressure crystallography

A flat crystal, 120 × 120 × 35 μm, was mounted in a diamond-anvil pressure cell for X-ray diffraction (Hazen and Finger, 1982), with a 4:1 methanol:ethanol mixture as the pressure medium and ruby fragments for pressure calibration. The (001) cleavage plate was secured parallel to one diamond-anvil face with a small dot of petroleum jelly. The eight-reflection centering procedure of King and Finger (1979) was used to determine unit-cell parameters at nine pressures from 1 bar to 45 kbar.

The structures of gillespite I at 1 bar and 9 kbar, and of gillespite II at 21 and 45 kbar (all at 25°C), were refined (R from 3.0 to 4.0%; weighted R from 2.4 to 4.2%, see Table 1) from three-dimensional intensity data collected on an automated four-circle diffractometer. Reflections from one octant of reciprocal space (sin $\theta/\lambda < 0.76$) were collected for gillespite at P = 1 bar, T = 25°C, and all accessible reflections (sin $\theta/\lambda < 0.70$) were collected for gillespite at high pressure and T = 25°C. Omega step scans were employed for all measurements, which were made with Nb-filtered molybdenum radiation. All intensities were corrected for specimen absorption and, when appropriate, diamond-cell absorption (gillespite μ_l = 74.9 to 81.3 cm^{-1}, depending on pressure). Corrections were also made for Lorentz and polarization effects. Data were averaged prior to least-squares refinement with program RFINE (Finger and Prince, 1975). Neutral scattering factors of Cromer and Mann (1968) and coefficients for anomalous scattering of Cromer and Liberman (1970) were used for all atoms.

Tetragonal gillespite I has six atoms in the asymmetric unit. Both 1 bar and 9 kbar refinements of this phase included an isotropic extinction correction and anisotropic temperature factors. Orthorhombic gillespite II has nine atoms in the asymmetric unit. Anisotropic temperature factors for the four cations and the very anisotropic O1 anion were refined, whereas isotropic temperature factors were assumed for the remaining four oxygen atoms. Conditions of refinement for gillespite at four pressures are recorded in Table 1, and refined positional

Table 1. Refinement conditions and refined extinction parameters for gillespite at 25°C at four pressures

	1 bar	9 kbar	21 kbar	45 kbar
Number of observations ($I > 2\sigma$)	752	235	288	302
μ_l (cm^{-1})	74.9	76.1	78.2	81.3
Weighted R (%)*	2.9	2.5	4.2	3.1
R (%)**	3.0	3.4	4.0	3.1
r* ($\times 10^5$)	0.7(1)†	1.7(3)	...	...

*Weighted $R = [\Sigma w(F_o - F_c)^2/\Sigma wF_o^2]^{1/2}$.
**$R = \Sigma\big||F_o| - |F_c|\big|/\Sigma|F_o|$.
†Parenthesized figures represent *esd*'s.

Table 2. Refined positional and thermal parameters for gillespite at 25°C at four pressures

Atom	x	y	z	β_{11}	β_{22}	β_{33}	β_{12}	β_{13}	β_{23}	B equiv.**
				Gillespite I (P = 1 bar)						
Ba	1/4	3/4	0	0.00498(4)***	0.00498(4)	0.00077(1)	0	0	0	1.02(1)
Fe	1/4	1/4	0.0919(1)	0.00240(7)	0.00240(7)	0.00138(3)	0	0	0	0.84(1)
Si	0.5196(1)	0.9354(1)	0.1549(1)	0.00259(10)	0.00262(3)	0.00096(3)	-0.00004(8)	0.00025(5)	-0.00025(5)	0.72(1)
O1	0.4740(4)	0.9740(4)	1/4	0.0144(4)	0.0144(4)	0.0017(1)	-0.0048(7)	0.0025(2)	-0.0025(2)	2.76(8)
O2	0.7228(3)	0.9966(3)	0.1375(1)	0.0032(3)	0.0088(4)	0.0017(1)	-0.0005(3)	-0.0000(1)	0.0007(2)	1.48(4)
O3	0.3905(3)	0.0265(3)	0.0902(2)	0.0057(4)	0.0039(3)	0.0026(1)	0.0015(3)	-0.0020(2)	-0.0004(2)	1.63(4)
				Gillespite I (P = 9 kbar)						
Ba	1/4	3/4	0	0.0060(1)	0.0060(1)	0.0017(2)	0	0	0	1.48(7)
Fe	1/4	1/4	0.0908(3)	0.0032(2)	0.0032(2)	0.0014(5)	0	0	0	0.95(15)
Si	0.5195(2)	0.9365(2)	0.1550(5)	0.0029(3)	0.0029(2)	0.0023(7)	-0.0005(2)	0.0001(3)	-0.0003(2)	1.2(2)
O1	0.4726(7)	0.9726(7)	1/4	0.015(2)	0.015(2)	0.007(4)	0.001(2)	0.005(1)	-0.005(1)	4.6(1.3)
O2	0.7232(5)	0.9978(6)	0.1358(8)	0.0030(8)	0.0099(8)	0.0042(13)	-0.0009(6)	-0.0005(6)	0.0016(7)	2.4(4)
O3	0.3907(6)	0.0292(6)	0.0926(9)	0.0085(9)	0.0060(8)	0.0001(15)	0.0009(6)	-0.0023(7)	0.0007(7)	1.4†
				Gillespite II (P = 21 kbar)						
Ba	0	0	-0.0267(4)	0.0042(2)	0.00051(2)	0.0056(13)	-0.0023(2)	0	0	1.1(1)
Fe	1/2	0	0.1846(9)	0.0026(4)	0.0027(3)	0.0048(28)	-0.0005(4)	0	0	0.8(2)
SiA	0.2186(8)	0.6865(6)	0.3276(23)	0.0033(7)	0.0029(6)	0.004(8)	0.0004(5)	-0.002(2)	0.000(2)	0.8(6)
SiB	0.1868(5)	0.2564(6)	0.2946(18)	0.0020(5)	0.0023(5)	0.016(5)	-0.0003(5)	0.001(1)	-0.002(1)	1.6(4)
O1	0.2628(22)	0.1829(20)	0.4741(76)	0.007(3)	0.009(3)	0.06(3)	0.0006(18)	-0.001(6)	-0.006(9)	6(3)
O2A	0.2146(12)	0.4763(13)	0.2761(36)	††						1.3(2)
O2B	0.9727(12)	0.2219(12)	0.2686(38)	††						1.4(2)
O3A	0.6285(13)	0.2241(14)	0.2400(43)	††						1.2(2)
O3B	0.2813(14)	0.1563(15)	0.1401(41)	††						1.0(2)
				Gillespite II (P = 45 kbar)						
Ba	0	0	-0.0324(2)	0.0036(1)	0.0043(1)	0.0016(9)	-0.0017(2)	0	0	0.7(1)
Fe	1/2	0	0.1840(6)	0.0026(3)	0.0021(2)	0.010(2)	-0.0003(4)	0	0	1.1(1)
SiA	0.2147(5)	0.6875(5)	0.3374(15)	0.0023(4)	0.0022(5)	0.0068(5)	0.0003(4)	-0.0006(11)	-0.0010(11)	0.9(4)
SiB	0.1872(4)	0.2542(5)	0.2874(13)	0.0023(4)	0.0021(4)	0.012(3)	-0.0002(4)	-0.0006(9)	-0.0011(9)	1.3(3)
O1	0.2704(15)	0.1813(15)	0.4504(45)	0.014(2)	0.012(2)	0.008(16)	0.003(2)	-0.003(4)	0.002(5)	2.6(13)
O2A	0.2065(9)	0.2634(10)	0.2634(22)	††						1.1(1)
O2B	0.9727(9)	0.2105(8)	0.2812(21)	††						1.0(2)
O3A	0.6231(10)	0.2256(10)	0.2404(25)	††						1.0(1)
O3B	0.2810(11)	0.1572(10)	0.1296(29)	††						0.8(1)

*Gillespite I coordinates are reported in the second setting for space group $P4/ncc$ (origin at $\bar{1}$). Previous refinements were reported in first setting (origin at $\bar{4}$), which is at -1/4,1/4,0 from $\bar{1}$.

**B equiv. $= 4/3\{\Sigma\Sigma\beta_{ij}\, a_i \cdot a_j\}$.

***Parenthesized figures represent *esd*'s.

†Atom O3 of gillespite I at 9 kbar is nonpositive definite; equivalent B was calculated by increasing β_{33} by 1/2 *esd*, from 0.0001 ± 0.0015 to 0.00085.

††Isotropic thermal parameters only.

and thermal parameters are listed in Table 2. Observed and calculated structure factors for the four sets of gillespite intensity data are recorded in Tables 3a to 3d.[2]

PT crystallography

A second gillespite single crystal was mounted in a diamond cell modified for high-temperature, single-crystal X-ray diffraction (Hazen and Finger, 1981a). Calcium fluoride was included in the mount as an internal pressure standard with a second gillespite crystal (Hazen and Finger, 1981b), and temperature was calibrated with a thermocouple that also served as the heating element of the *PT* cell. In the *PT* cell the gillespite transition was always marked by twinning and consequent splitting and intensity loss for reflections from the high-pressure phase. It was thus not possible to obtain precise lattice parameters of gillespite II at high pressures and temperatures. Furthermore, boron carbide backing disks of the *PT* cell fractured above 25 kbar at 250°C, and reversals of the transition above 160°C were not completed. The *PT* data obtained, however, were sufficient to define isochores for gillespite I and to bracket the gillespite I–II transition below 200°C.

Results

Gillespite lattice variations with pressure and temperature

Unit-cell parameters of gillespite I and II at nine pressures at 25°C are recorded in Table 4, and variations in these cell parameters with pressure are illustrated in Figure 2. The bulk modulus of gillespite I, calculated from four unit-cell measurements between 1 bar and 18.5 kbar, is 0.62±0.03 Mbar. The *c* dimension is amost twice as compressible as the *a* dimension. The bulk modulus of gillespite II, calculated from five points between 17.6 and 45.3 kbar, is 0.66±0.03 Mbar. The *c* dimension of the orthorhombic phase is also significantly more compressible than *a* or *b*.

At room temperature the natural gillespite I–II transition is bracketed at 18±1 kbar; the two phases may

[2] To obtain a copy of Tables 3a to 3d, order Document AM-83-223 from the Business Office, Mineralogical Society of America, 2000 Florida Avenue, N.W., Washington, D.C. 20009. Please remit $1.00 in advance for the microfiche.

Table 4. Unit-cell parameters of gillespite I and II under nine high-pressure (at 25°C) and fourteen *PT* conditions

P (kbar)	*T* (°C)	*a* (Å)	*b* (Å)	*c* (Å)	*V* (Å^3)	Phase I or II	Remarks
0.001	25	7.5161(3)*	7.5160(3)	16.0759(7)	908.18(6)	I	In air**
9.3(5)	25	7.493(1)	7.491(1)	15.943(2)	894.9(1)	I	In pressure cell**
20.6(5)	25	7.5001(5)	7.3223(4)	7.921(1)	435.00(7)	II	In pressure cell**
45.3(5)	25	7.445(1)	7.224(1)	7.783(1)	418.59(7)	II	in pressure cell**
29.7(5)	25	7.4778(6)	7.2826(6)	7.8663(6)	428.38(6)	II	in pressure cell**
15.0(5)	25	7.4754(5)	7.4749(5)	15.867(1)	886.5(1)	I	In pressure cell**
18.5(5)	25	7.464(5)	7.457(5)	15.811(1)	880.0(6)	I	In pressure cell**
17.6(5)	25	7.5035(5)	7.3315(5)	7.9320(6)	436.36(5)	II	In pressure cell**
20.8(5)	25	7.4985(5)	7.3223(5)	7.920(1)	434.84(7)	II	In pressure cell**
22.5	60	∿7.43				II	In *PT* cell†
20.3	85	∿7.44				II	In *PT* cell†
10.4	115	7.491(1)	7.491(1)	15.958(2)	447.66(9)	I	In *PT* cell
4.0	150	7.497(5)	7.498(5)	16.032(12)	450.5(5)	I	In *PT* cell
6.6	170	7.498(5)	7.498(5)	16.04(2)	450.6(7)	I	In *PT* cell
5.6	195	7.499(5)	7.496(6)	16.040(14)	450.8(6)	I	In *PT* cell
7.4	235	7.498(5)	7.499(5)	16.046(12)	451.1(5)	I	In *PT* cell
7.3	285	7.513(7)	7.510(8)	16.04(2)	452.7(8)	I	In *PT* cell
22.2	150	∿7.43				II	In *PT* cell†
20	150	∿7.45				II	In *PT* cell†
17.4	150	7.475(10)	7.480(8)	15.86(2)	442.9(8)	I	In *PT* cell
0.001	28	7.516(4)	7.513(5)	16.075(14)	453.9(5)	I	In *PT* cell
0.001	115	7.516(5)	7.515(6)	16.085(16)	454.2(7)	I	In *PT* cell
0.001	275	7.517(4)	7.517(5)	16.10(2)	454.9(6)	I	In *PT* cell

*Parenthesized figures represent *esd*'s.
**Data collection under these conditions.
†Gillespite II was twinned under these *PT* conditions and complete unit-cell parameters could not be resolved.

coexist (one metastably) over a small pressure region between 17 and 19 kbar. This transition pressure for natural gillespite from California is intermediate between the previously reported values of 12±1 kbar for synthetic material (Huggins *et al.*, 1976) and the approximate measurement of 26 kbar for a different natural sample (Strens, 1966). The transition pressures of 12 and 18 kbar were determined with the same calibration technique. Differences between synthetic and natural samples (see Discussion, below), rather than calibration errors, could account for most of the observed differences.

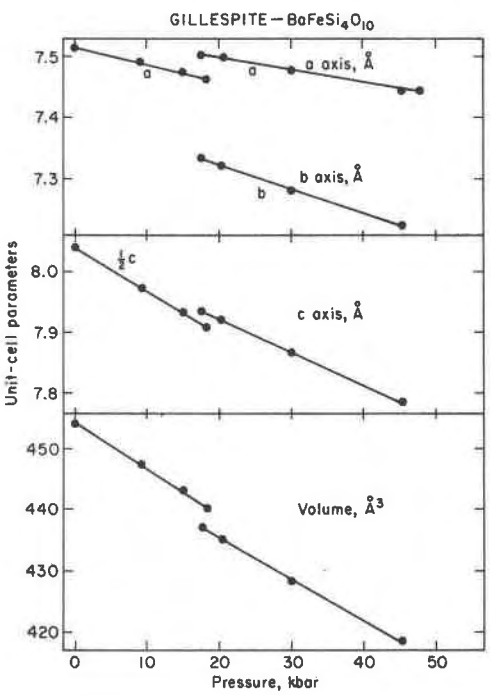

Fig. 2. Variation of gillespite unit-cell parameters versus pressure. The gillespite I–II transition at 25°C is bracketed at 18±1 kbar.

Unit-cell parameters measured under fourteen *PT* conditions (Table 4) may be used to determine gillespite thermal expansion coefficients, the gillespite I–II transition boundary in the *P–T* plane, and isochores (lines of constant volume). Axial thermal expansion of gillespite I is extremely anisotropic. The coefficient of expansion in the *c* direction is $6.0\pm2.0\times10^{-6}$ °C^{-1}, whereas the coefficient of expansion in a direction perpendicular to *c* is $0.0\pm1.0\times10^{-7}$ °C^{-1}. The gillespite phase transition was reversed at 85°C (19.5±1 kbar), at 160°C (21.5±1.5 kbar), and at room temperature (18±1 kbar). The Clausius–Clapeyron slope (27±9 bar/°C) is thus positive, as predicted by Hazen and Finger (1979). Figure 3, which illustrates the gillespite I–II transition, is a nomogram of unit-cell volume versus temperature and pressure. The positive *P–T* slopes of gillespite-I isochores are approximately equal to the transition slope.

Crystal structures of gillespite I and II

Selected interatomic distances and angles of gillespite I and II (Table 5) reveal several significant variations of crystal structure with pressure. In both forms the average of all Si–O distances is approximately 1.60±0.01Å; there is no significant compression of the silicon tetrahedra within experimental error, though a small but real com-

Table 5. Selected interatomic distances and bond angles for gillespite I and II at 25°C at four pressures

Gillespite I					
Bond	1 bar	9 kbar	Angle	1 bar	9 kbar
Si-O1	1.594(1)*	1.578(7)	O1-Si-O2	108.5(2)	110.0(6)
Si-O2	1.620(2)	1.623(5)	O1-Si-O2	109.2(2)	109.3(6)
Si-O2	1.627(2)	1.632(5)	O1-Si-O3	114.9(1)	113.6(6)
Si-O3	1.578(2)	1.551(11)	O2-Si-O2	108.6(2)	108.5(4)
Mean Si-O	1.605	1.596	O2-Si-O3	105.5(1)	105.5(5)
			O2-Si-O3	110.0(1)	109.7(6)
Si-Si	3.187(2)	3.153(14)	Si-O1-Si	177.4(3)	175.8(6)
Si-Si [2]**	3.144(1)	3.141(3)	Si-O2-Si	151.1(2)	149.6(7)
Fe-O3 [4]	1.985(2)	1.962(5)	O3-Fe-O3	178.5(2)	178.4(9)
			O3-Fe-O3	90	90
Ba-O2 [4]	2.925(2)	2.880(9)			
Ba-O3 [4]	2.747(2)	2.768(9)			
Mean Ba-O	2.836	2.824			

Gillespite II					
Bond	21 kbar	45 kbar	Angle	21 kbar	45 kbar
SiA-O1	1.577(54)	1.606(30)	O1-SiA-O2A	103.9(15)	109.1(9)
SiA-O2A	1.592(13)	1.639(11)	O1-SiA-O2B	111.4(14)	109.6(8)
SiA-O2B	1.652(14)	1.637(9)	O1-SiA-O3A	113.7(15)	116.3(9)
SiA-O3A	1.491(21)	1.556(14)	O2-SiA-O2B	107.7(9)	107.2(6)
Mean SiA-O	1.58	1.61	O2A-SiA-O3A	108.7(12)	103.6(8)
			O2B-SiA-O3A	111.0(11)	110.5(8)
SiB-O1	1.624(57)	1.557(33)	O1-SiB-O2A	111.2(14)	114.0(10)
SiB-O2A	1.631(11)	1.614(9)	O1-SiB-O2B	113.8(14)	111.9(9)
SiB-O2B	1.638(10)	1.629(7)	O1-SiB-O3B	111.4(12)	108.6(9)
SiB-O3B	1.593(30)	1.577(21)	O2A-SiB-O2B	105.4(6)	106.0(4)
Mean SiB-O	1.62	1.59	O2A-SiB-O3B	109.2(12)	108.1(8)
			O2B-SiB-O3B	105.6(13)	109.0(8)
SiA-SiB (11*c*)	3.118(17)	3.049(12)	SiA-O1-SiB (11*c*)	153.4(14)	149.1(11)
SiA-SiB (11*a*)	3.169(7)	3.161(5)	SiA-O2A-SiB (11*a*)	159.2(6)	152.7(13)
SiA-SiB (11*b*)	3.080(6)	3.046(5)	SiA-O2B-SiB (11*b*)	138.9(13)	137.7(6)
Fe-O3A [2]	1.953(12)	1.921(8)	O3A-Fe-O3A	154.0(20)	153.6(12)
Fe-O3B [2]	2.031(12)	2.031(9)	O3A-Fe-O3B	88.0(5)	87.5(3)
Fe-O1 [2]	3.197(43)	2.989(25)	O3A-Fe-O3B	96.5(4)	98.0(3)
Mean of 4 Fe-O	1.992	1.976	O3B-Fe-O3B	160.0(18)	155.9(12)
Mean of 6 Fe-O	2.394	2.314			
Ba-O2A [2]	2.918(20)	2.835(12)			
Ba-O2B [2]	2.855(26)	2.883(15)			
Ba-O3A [2]	2.805(22)	2.718(14)			
Ba-O3B [2]	2.740(18)	2.694(12)			
Ba-O3B [2]	3.136(13)	3.059(9)			
Mean of 8 Ba-O	2.830	2.783			
Mean of 10 Ba-O	2.891	2.838			

*Parenthesized figures represent *esd*'s.
**Bracketed figures represent bond multiplicity.

pression of Si–O bonds would be consistent with the data. Uncertainties in oxygen positions have a large effect on individual Si–O distances; thus estimated standard deviations of these Si–O distances in the high-pressure refinements are as large as 0.06Å. For all tetrahedra at all pressures, however, the bonds between Si and bridging O2 (within the four-membered tetrahedral rings) are longer than Si–O3 (nonbridging) and Si–O1 (bridging, between four-membered rings) bonds. These systematic differences in Si–O distance reflect both the Si–O–Si angles and the degree of bond saturation (Hazen and Burnham, 1974).

Significant changes occur in Si–O–Si angles (and consequently in Si–Si distances) as a result of the gillespite I–II transition. The low-pressure phase is notable for its nearly linear Si–O1–Si bonds (177°). These inter-ring angles, which represent the tetrahedral tilting between adjacent four-membered rings of tetrahedra, are defined by atoms aligned approximately along the *c* axis. The intra-ring Si–O2–Si angles in gillespite I, which lie near the (001) plane, are approximately 151°. A significant change in the transition from gillespite I to II is the "kinking" of the Si–O1–Si bond angle to approximately 153°.

The ferrous iron coordination square of gillespite I undergoes significant compression, though no distortion, between 1 bar and 9 kbar. Linear compressibility, β_l, of the Fe–O3 bonds in square-planar coordination, based on the 1-bar and 9-kbar points, is approximately 1.3×10^{-3} $kbar^{-1}$. In gillespite II this site is significantly distorted from square-planar coordination to an extremely flattened tetrahedral configuration. The average distance of

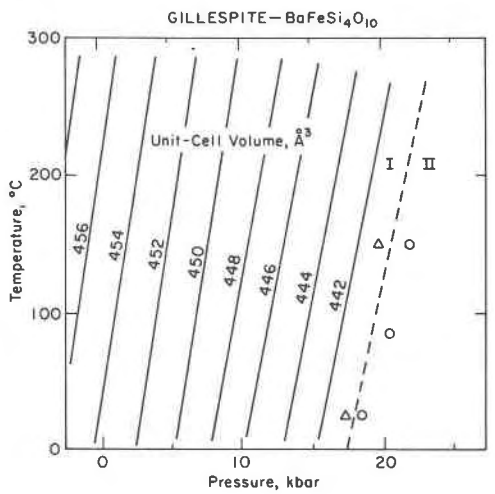

Fig. 3. Nomogram of gillespite unit-cell volume (subcell volume in the case of gillespite I) versus pressure and temperature. The gillespite I–II transition (dashed line) is marked by a volume discontinuity but little change in compressibility. Circles represent transitions from gillespite I to II; triangles represent reversals of gillespite II to I.

the four Fe–O bonds *increases* at the 18-kbar transition by more than 2%. Such an increase in bond distance at high pressure is commonly the consequence of an increase in cation coordination number (*e.g.*, Shannon, 1976). Two additional long (3.2Å) Fe–O distances, which are the 5th and 6th nearest neighbors to Fe in gillespite II, are not observed in gillespite I. Furthermore, these two long Fe–O1 bonds are extremely compressible; between 21 and 45 kbar the Fe–O1 bonds compress 6.5%, compared with less than 1% compression for the average Fe–O3 bond. These variations of the iron coordination group with pressure may help to explain the changing character of the Mössbauer spectra above 30 kbar.

The barium atom of gillespite I has eight-fold distorted cubic coordination with four Ba–O3 bonds of 2.747Å and four Ba–O2 bonds of 2.925Å under room conditions. At 9 kbar the barium–oxygen distances become more uniform, with Ba–O2 bonds compressing to 2.880Å ($\beta_l = 1.7\times10^{-3}$ kbar^{-1}) and Ba–O3 bonds expanding to 2.768Å ($\beta_l = -0.8\times10^{-3}$ kbar^{-1}). The average of eight Ba–O bond distances extrapolated to 18 kbar, just above the gillespite I–II transition, is 1.0% *greater* than below the transition. This fact is suggestive, once again, of an increase in cation coordination. In fact, two more Ba–O3 bonds, which are slightly longer than 3Å, are found in the high-pressure form. Furthermore, between 21 and 45 kbar these longer Ba–O3 bonds ($\beta_l = 1.0\times10^{-3}$ kbar^{-1}) are more compressible than the average of the eight shorter bonds ($\beta_l = 0.7\times10^{-3}$ kbar^{-1}). The significant differences between barium coordination polyhedra in gillespite I and II are illustrated in Figure 4.

Thermal vibration ellipsoids

Orientations and magnitudes of thermal vibration ellipsoids of gillespite are reported in Table 6, and equivalent isotropic temperature factors appear in Table 2. Values for gillespite I do not differ significantly from those reported by Hazen and Burnham (1974); anisotropic thermal parameters of gillespite II were not determined in the previous study. In both phases of gillespite, the 2-coordinated bridging O1 oxygen between adjacent four-membered rings of tetrahedra has an unusually large, anisotropic vibration ellipsoid. The maximum vibration direction is perpendicular to the Si–O1–Si bonds for all conditions studied. In gillespite I, which has nearly straight Si–O1–Si bond angle of 177°, the large vibration amplitude perpendicular to the bond may represent a time-averaged position of a vibrating atom that is usually not centered between the two Si atoms (Liebau, 1961). Molecular orbital calculations (Gibbs *et al.*, 1982), however, indicate that straight Si–O–Si bonds may not be as energetically unfavorable as once thought.

Discussion

Lattice variations of gillespite with temperature and pressure

Gillespite, like other layer minerals, displays extremely anisotropic compressibility and thermal expansivity. In both phases of gillespite, compression parallel to *c* is approximately twice the compression parallel to the (001) plane; as similarly found in micas and chlorites (Hazen and Finger, 1978). The same anisotropy is observed at high temperature; thermal expansion parallel to *c* is much greater than expansion parallel to the (001) plane.

In gillespite, as in all layer minerals, the sheet-like cleavage and other anisotropic physical properties are consequences of nonuniform bonding forces. Intralayer bonds, such as Si–O in silicates or C–C in graphite, are much stronger than interlayer bonds, such as alkali–oxygen or Van der Waals bonds. Interlayer compression and expansion, therefore, are generally greater than intralayer compression and expansion. In gillespite, for example, dimensional changes within the (001) plane of silicate layers are controlled by the corner-linked silicon tetrahedral sheets, whereas dimensional changes perpendicular to the layers are controlled by shortening of the less rigid barium–oxygen bonds.

The gillespite I–II transition

The gillespite I–II phase transition displays aspects of both displacive and reconstructive phase transformations. The transition is primarily displacive, for it occurs rapidly and reversibly, and crystals, either single or twinned, remain euhedral through the transition. The transition does involve a significant volume discontinuity, however, and the primary coordination spheres of several atoms (most notably barium) are altered. In some re-

Table 6. Magnitudes and orientations of thermal ellipsoids for gillespite at 25°C at four pressures

Gillespite I		1 bar				9 kbar			
Atom	Axis	rms displacement (Å)	Angle with respect to: a (°)	b (°)	c (°)	rms displacement (Å)	Angle with respect to: a (°)	b (°)	c (°)
Ba	r_1	0.1006(7)*	90	90	0	0.1312(5)	90	0	90
	r_2	0.1194(3)	0	90	90	0.1312(5)	0	90	90
	r_3	0.1194(3)	90	0	90	0.1478(9)	90	90	0
Fe	r_1	0.0828(12)	0	90	90	0.096(2)	0	90	90
	r_2	0.0828(12)	90	0	90	0.096(2)	90	0	90
	r_3	0.1344(14)	90	90	0	0.133(22)	90	90	0
Si	r_1	0.082(2)	45(20)	128(21)	110(2)	0.082(5)	47(10)	43(10)	87(3)
	r_2	0.086(2)	131(21)	139(20)	91(8)	0.098(4)	137(10)	48(10)	86(5)
	r_3	0.116(2)	76(2)	104(2)	20(2)	0.172(26)	89(4)	95(4)	5(4)
O1	r_1	0.109(7)	108(1)	72(1)	27(2)	0.114(51)	128(6)	52(6)	60(14)
	r_2	0.166(6)	135	135	90	0.216(14)	135	135	90
	r_3	0.256(6)	51(1)	129(1)	63(2)	0.341(67)	69(9)	111(9)	30(14)
O2	r_1	0.095(5)	6(4)	85(3)	92(4)	0.090(12)	7(5)	84(6)	88(6)
	r_2	0.138(4)	86(4)	56(5)	146(5)	0.158(10)	85(7)	20(10)	99(11)
	r_3	0.168(4)	94(2)	34(5)	56(5)	0.240(31)	94(5)	71(11)	19(11)
O3	r_1	0.088(5)	47(6)	134(8)	104(4)	0.033**	59	108	36
	r_2	0.115(4)	125(7)	135(8)	114(3)	0.136	99	163	105
	r_3	0.203(4)	117(2)	82(2)	28(2)	0.181	32	90	122

Gillespite II		21 kbar				45 kbar			
Atom	Axis	rms displacement (Å)	Angle with respect to: a (°)	b (°)	c (°)	rms displacement (Å)	Angle with respect to: a (°)	b (°)	c (°)
Ba	r_1	0.080(4)	41(1)	49(1)	90	0.070(19)	90	90	0
	r_2	0.133(15)	90	90	0	0.079(3)	139(1)	131(1)	90
	r_3	0.139(2)	131(1)	41(1)	90	0.124(2)	131(1)	41(1)	90
Fe	r_1	0.077(8)	45(15)	45(15)	90	0.073(6)	68(21)	22(21)	90
	r_2	0.093(7)	45(15)	135(15)	90	0.087(6)	158(21)	68(21)	90
	r_3	0.123(36)	90	90	0	0.173(18)	90	90	0
SiA	r_1	0.072(44)	41(30)	115(62)	60(62)	0.072(10)	111(65)	22(56)	83(21)
	r_2	0.092(15)	110(72)	154(61)	106(20)	0.079(10)	158(61)	110(66)	100(14)
	r_3	0.132(72)	124(58)	92(25)	34(58)	0.147(55)	97(12)	100(15)	12(16)
SiB	r_1	0.072(11)	34(82)	56(82)	90(14)	0.069(10)	61(29)	30(28)	83(5)
	r_2	0.077(11)	57(83)	146(81)	98(5)	0.082(8)	151(29)	61(29)	90(5)
	r_3	0.226(35)	86(5)	97(5)	8(5)	0.191(28)	93(5)	96(5)	7(5)
O1	r_1	0.142(25)	23(63)	113(63)	92(10)	0.127(115)	63(37)	118(58)	41(74)
	r_2	0.157(25)	113(63)	156(62)	96(7)	0.187(53)	85(86)	145(38)	124(49)
	r_3	0.46(12)	91(6)	96(8)	6(8)	0.216(24)	28(21)	71(45)	109(62)

*Parenthesized figures represent *esd*'s.

**Atom O3 of gillespite I at 9 kbar was nonpositive definite. Thermal ellipsoid for this atom was calculated after β_{33} was increased by 1/2 *esd*, from 0.0001 ± 0.0015 to 0.00085.

spects, therefore, gillespite illustrates the difficulty in classifying phase transitions on the basis of physical or structural criteria.

Hazen (1977) and Hazen and Finger (1979) described the gillespite I–II transition as a geometrically controlled phenomenon, in which the relative sizes of barium polyhedra and silicate layers play a key role. The barium polyhedron expands with temperature and compresses with pressure, whereas the silicate layers are relatively unaffected by changes in P and T. At atmospheric pressure barium–oxygen bonds form a distorted cubic coordination polyhedron, causing a spacing of 4.5Å between silicate layers. At some critical size ratio, perhaps defined by the transition at 18 kbar and 25°C, the barium–oxygen distances become too small to support this relatively wide interlayer separation in gillespite I, and the barium coordination polyhedron collapses, resulting in an interlayer spacing of less than 4.0Å in gillespite II. The similarity of isochore and Clausius–Clapeyron slopes is further evidence for a geometrically controlled transition.

"Gillespite III" and high-pressure Mössbauer spectra

Huggins *et al.* (1976) collected high-pressure Mössbauer data and examined optical properties of synthetic $BaFeSi_4O_{10}$ to 142 kbar. They proposed the existence of a third phase, "gillespite III," on the basis of a color change from blue to colorless, and the presence of a

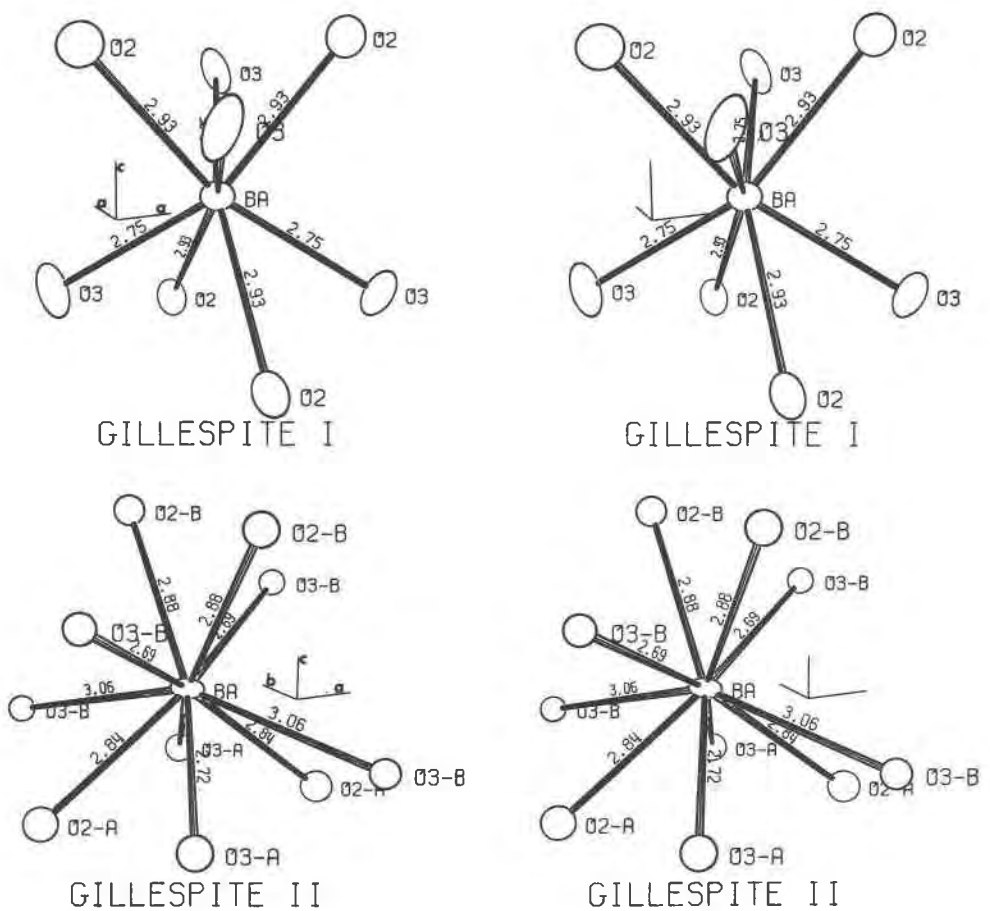

Fig. 4. Stereoscopic pairs of barium polyhedra in gillespite I and gillespite II.

second doublet in the Mössbauer spectrum near 70 kbar. Subsequent study by Huggins, Mao and Virgo (D. Virgo, pers. comm.) has not substantiated this hypothesis. The color change is gradual from blue to colorless, and the second Mössbauer doublet is present at *all* pressures from 1 bar to 142 kbar (the intensity of the weaker doublet increases with pressure). Furthermore, new X-ray powder diffraction data on synthetic gillespite at 142 kbar (D. Virgo, pers. comm.) yield an orthorhombic unit cell (a = 7.32, b = 6.94, c = 7.49Å) that is consistent with an extrapolation of gillespite II unit-cell data from this single-crystal study. There is no evidence for the existence of gillespite III.

The origin of the second Mössbauer doublet in synthetic gillespite remains a puzzle. In the natural specimen iron is observed to occupy only one site, the square-planar site: only one Mössbauer doublet should appear. We suggest that a few percent Fe^{2+} has entered the Ba site in the synthetic gillespite used by Huggins *et al.* (1976), thus causing a second weak doublet in the spectrum. With increasing pressure, the distortions of the Ba polyhedron, combined with increased preferred orientation of platelets in gillespite powder, could result in a systematic change in doublet intensity ratios.

Differences in the measured I–II transition pressure of natural (18 kbar) versus synthetic (12 kbar) gillespite might also be a consequence of iron in the barium site. A few percent ferrous iron would reduce the size of the barium polyhedron, and thus lower the pressure of the structurally-controlled gillespite I–II transition. Synthesis and X-ray study of gillespite single crystals, combined with Mössbauer spectra of natural gillespite, might help to resolve these aspects of gillespite crystal chemistry.

Concluding statement

Reversible phase transitions are common in many silicates and silicate-type structures, yet they are difficult to study, for by definition these transitions are nonquenchable. *In situ* experiments under high-temperature *and* high-pressure conditions are essential for the documentation of the structures and stabilities of such phases. In spite of the experimental difficulties, the study of reversible transitions is an essential part of mineralogy because the physical properties of common feldspars, feldspath-

oids, silica minerals, pyroxenes, zeolites, and other minerals, as well as the rocks that contain them, may be greatly altered by slight structural changes associated with displacive transitions. Electrical, magnetic, and elastic properties of minerals may vary significantly and discontinuously across displacive transitions. In gillespite, for example, the displacive phase change is marked by a dramatic discontinuity in optical absorption, which is correlated to the changes in the crystal field of iron. Microstructural properties of minerals, including twinning, exsolution, and cation ordering, may differ depending on the symmetry history of the phase. Twinning in gillespite, for example, is commonly induced by the symmetry reduction of the I to II transition. Application of *PT* crystallography to the study of mineral systems thus will be an important element in efforts to identify and describe phase transitions in minerals.

Acknowledgments

The authors gratefully acknowledge thoughtful and constructive reviews of this study by H. Belsky, F. Chayes, C. T. Prewitt, M. Ross, D. Virgo, and H. S. Yoder, Jr. D. Virgo also provided access to unpublished high-pressure Mössbauer and powder diffraction data on synthetic $BaFeSi_4O_{10}$. This research was supported in part by the National Science Foundation Grant EAR81-15517.

References

Abu-Eid, R. M., Mao, H. K., and Burns, R. G. (1973) Polarized absorption spectra of gillespite at high pressure. Carnegie Institution of Washington Year Book, 72, 564–567.

Cromer, D. T. and Liberman, D. (1970) Relativistic calculations of anomalous scattering factors for X-rays. Journal of Chemical Physics, 53, 1891–1898.

Cromer, D. T. and Mann, J. B. (1968) X-ray scattering factors computed from numerical Hartree–Fock wave functions. Acta Crystallographica, A24, 321–324.

Finger, L. W. and Prince, E. (1975) A system of Fortran IV computer programs for crystal structure computations. National Bureau of Standards (United States) Technical Note, 854.

Gibbs, G. V., E. P. Meagher, M. D. Newton, and D. K. Swanson (1982) A comparison of experimental and theoretical bond length and angle variations for minerals, inorganic solids, and molecules. In M. O'Keeffe and A. Navrotsky Eds., Structure and Bonding in Crystals, p. 195–225. Academic Press, New York.

Hazen, R. M. (1977) Mechanisms of transformation and twinning in gillespite at high pressure. American Mineralogist, 62, 528–533.

Hazen, R. M. and Burnham, C. W. (1974) The crystal structures of gillespite I and II: a structure determination at high pressure. American Mineralogist, 59, 1166–1176.

Hazen, R. M. and Burnham, C. W. (1975) The crystal structure of gillespite II: correction and addendum. American Mineralogist, 60, 937–938.

Hazen, R. M. and Finger, L. W. (1978) The crystal structures and compressibilities of layer minerals at high pressure. II. Phlogopite and chlorite. American Mineralogist, 63, 293–296.

Hazen, R. M. and Finger, L. W. (1979) Polyhedral tilting: a common type of pure displacive phase transition and its relationship to analcite at high pressure. Phase Transitions, 1, 1–22.

Hazen, R. M. and Finger, L. W. (1981a) High-temperature diamond-anvil pressure cell for single-crystal studies. Review of Scientific Instruments, 52, 75–79.

Hazen, R. M. and Finger, L. W. (1981b) Calcium fluoride as an internal pressure standard in high-pressure/high-temperature crystallography. Journal of Applied Crystallography, 14, 234–236.

Hazen, R. M. and Finger, L. W. (1982) Comparative Crystal Chemistry. Wiley, New York.

Huggins, F. E., Mao, H. K., and Virgo, D. (1975) Mössbauer studies at high pressure using the diamond-anvil cell. Carnegie Institution of Washington Year Book, 74, 405–410.

Huggins, F. E., Mao, H. K., and Virgo, D. (1976) Gillespite at high pressure: results of a detailed Mössbauer study. Carnegie Institution of Washington Year Book, 75, 756–758.

King, H. E. and Finger, L. W. (1979) Diffracted beam crystal centering and its application to high-pressure crystallography. Journal of Applied Crystallography, 12, 374–378.

Liebau, F. (1961) Untersuchungen über die groösse des Si–O–Si-valenzwinkels. Acta Crystallographica, 14, 1103–1109.

Shannon, R. D. (1976) Revised effective ionic radii and systematic studies of interatomic distances in halides and chalcogenides. Acta Crystallographica, A32, 751–767.

Strens, R. G. J. (1966) Pressure-induced spin-pairing in gillespite, $BaFe(II)Si_4O_{10}$. Chemical Communications, 21, 777–778.

Manuscript received, August 2, 1982;
accepted for publication, December 1, 1982.